OAK RIDGE NATIONAL LABORATORY
operated by
UNION CARBIDE CORPORATION
NUCLEAR DIVISION
for the
U.S. ATOMIC ENERGY COMMISSION

ORNL-TM-1456

CREEP-RUPTURE PROPERTIES OF FS-85 ALLOY AND THEIR RESPONSE TO HEAT TREATMENT

R. L. Stephenson

ORNL-TM-1456

Contract No. W-7405-eng-26

METALS AND CERAMICS DIVISION

CREEP-RUPTURE PROPERTIES OF FS-85 ALLOY AND THEIR RESPONSE TO HEAT TREATMENT

R. L. Stephenson

JULY 1966

OAK RIDGE NATIONAL LABORATORY
Oak Ridge, Tennessee
operated by
UNION CARBIDE CORPORATION
for the
U.S. ATOMIC ENERGY COMMISSION

CREEP-RUPTURE PROPERTIES OF FS-85 ALLOY AND THEIR RESPONSE TO HEAT TREATMENT

R. L. Stephenson

ABSTRACT

Creep-rupture properties for FS-85 (Nb–27% Ta–10% W–1% Zr) to 1000 hr are presented at 982°C (1800°F), 1093°C (2000°F), 1204°C (2200°F), and 1427°C (2600°F). Substantial improvements in strength at 982°C (1800°F) and 1204°C (2200°F) can be achieved by pretest annealing 1 hr at 1593°C (2900°F). These improvements are shown to be stable for at least 1000 hr. Pretest annealing at higher temperatures yields inferior properties. A tentative explanation for these effects is offered in terms of precipitate distribution.

INTRODUCTION

A large number of refractory-metal alloys are currently under consideration for high-temperature structural applications. In most cases, the only mechanical property data available on these materials are tensile test data and very short-time creep data. Since long-time creep properties are important for many high-temperature applications, an evaluation of several promising refractory-metal alloys was undertaken. This evaluation included the determination of creep properties to 1000 hr, so that a valid comparison of the suitability of the alloys for high-temperature structural applications could be made. This report describes such an evaluation of FS-85 alloy (Nb–27% Ta–10% W–1% Zr).

MATERIAL

The material used in this study was obtained from Westinghouse Corp. as Heat No. 850738-T1. The vendors' analysis is as follows:

Element	Weight Percent
Tantalum	27.73
Tungsten	10.15
Zirconium	0.83
Carbon	0.0080
Oxygen	0.0041
Nitrogen	0.0029
Niobium	balance

In the preparation of this material, a vacuum arc-melted ingot was forged from 1325°C (2415°F) to a 2 7/8 in. thickness. The forging was conditioned, reheated to 1300°C (2372°F) and forged to a 1 1/2-in. thickness. The material was then vacuum annealed 1 hr at 1500°C (2732°F), transferred to an argon furnace, heated to 1250°C (2282°F), and forged to an 0.7-in. thickness. It was then rolled (with an appropriate cross rolling to control width) from 315°C (598°F), reheated to 204°C (400°F) and rolled to final gage. The sheet was given a recrystallization anneal of 1 hr at 1371°C (2500°F), then roller leveled.

EXPERIMENTAL DETAILS

The apparatus used in this work is described in a previous report.[1] The tests were performed at pressures lower than 2×10^{-7} torr. Every test specimen was analyzed for interstitials. The after-test oxygen content of most specimens was between 100 and 300 ppm. The metallographic specimens were prepared by vibratory polishing in the manner described by Long and Gray.[2]

RESULTS AND DISCUSSION

The creep-rupture properties of as-received FS-85 alloy at 980°C (1800°F) are given in Fig. 1. Times to 1, 2, and 5% elongation are

---

[1] R. L. Stephenson, Comparative Creep-Rupture Properties of D-43 and B-66 Alloys, ORNL-TM-944 (November 1964).

[2] E. L. Long and R. J. Gray, Metals Progr. 74(4), 145–48 (1958).

plotted as a function of stress along with the time to rupture. Similarly, the creep-rupture properties at 1093°C (2000°F), 1204°C (2200°F), and 1427°C (2600°F) are given in Figs 2, 3, and 4, respectively. (The time to 10% elongation is included in these three figures.) Figure 5 shows the secondary creep rate as a function of stress for each of these four temperatures. Isochronous stress-strain curves for FS-85 at all four temperatures are shown in Figs. 6, 7, 8, and 9, respectively. It can be seen from Figs. 3 and 4 that at long times and high temperatures the curves exhibit a pronounced curvature. The ductilities seem to be adequate at all of the temperatures investigated, the lowest being an average of approximately 19% for the 982°C (1800°F) tests.

In order to determine the effect of annealing temperature on the creep-rupture properties, duplicate specimens were annealed at various temperatures. After annealing, one specimen from each pair was loaded to 35,000 psi at 982°C (1800°F) while the other was loaded to 17,500 psi at 1204°C (2200°F). The times to selected percent elongations and to rupture are plotted as a function of pretest annealing temperature for the 982°C (1800°F) tests in Fig. 10. Figure 11 gives the influence of pretest annealing temperature on the properties at 1204°C (2200°F). The influence of pretest annealing temperature on the secondary creep rate at 982°C (1800°F) and 1204°C (2200°F) is shown in Fig. 12. It can be seen that the creep-rupture properties can be improved substantially by annealing at moderately high temperatures while annealing at still higher temperatures yields inferior properties. In order to determine the long-time stability of these improvements, a number of specimens were annealed at 1593°C (2900°F), the apparent optimum temperature, and tested at 982°C (1800°F) and 1204°C (2200°F). The results of these experiments are shown in Figs. 13 and 14. (Curves showing the time to 1% creep and to rupture for the as-received material are included for comparison.) Isochronous stress-strain curves for the pretest annealed material at 982°C (1800°F) and 1204°C (2200°F) are shown in Figs. 15 and 16, respectively. Annealed specimens tested at 982°C (1800°F) average approximately 11% ductility.

A possible explanation for the effect of pretest annealing temperature on the mechanical properties and for the severe curvature of the creep-rupture curves (Figs. 3 and 4) at high temperatures is suggested by the microstructures of the creep specimens. Figure 17 shows the microstructures of specimens tested at 982°C (1800°F). Figure 17a shows a representative view of the microstructure at high magnification and a view of the fracture at low magnification of a specimen tested a very short time. Figure 17b shows similar views of a specimen tested for a long time at the same temperature. Analogous views of short- and long-time specimens tested at 1093°C (2000°F), 1204°C (2200°F), and 1427°C (2600°F) are shown in Figs. 18, 19, and 20, respectively. All specimens give some indication, however inconclusive, of a precipitate. At longer times and higher temperatures a precipitate is distinctly visible in the grain boundaries. At 1204°C (2200°F) the appearance of this precipitate in the grain boundaries is roughly concurrent with the onset of curvature in the curve of time to reach 1% creep vs stress. Figure 21 shows photomicrographs of specimens tested at 982°C (1800°F) and 1204°C (2200°F) after a pretest anneal of 1 hr at approximately 1760°C (3200°F). In contrast to the specimens shown in the preceding figures, which showed substantial fracture ductility, these specimens are seen to fail intergranularly with very little deformation of the matrix material. It is possible that increasing pretest annealing temperatures places progressively more of this precipitate in solution, allowing it to reprecipitate in a finely dispersed state at the test temperature and hence produce the higher strength properties. At still higher temperatures it is possible that increased atom mobilities allow more rapid coalescence of the remaining precipitate in the grain boundaries while grain growth reduces the grain boundary area and thus decreases the amount of precipitate needed to cause significantly reduced fracture ductility.

Precipitates that are identical in appearance have been observed in D-43 (Nb–10% W–1% Zr–0.1% C) and Cb-752 (Nb–10% W–2.5% Zr) also.[3]

---

[3]R. L. Stephenson, to be published.

Attempts have been made to identify this precipitate by electron diffraction.[4] The results are inconclusive but preliminary data indicate that it is ZrO_2.

SUMMARY

The creep-rupture properties have been determined to 1000 hr for a heat of FS-85 alloy at 982°C (1800°F), 1093°C (2000°F), 1204°C (2200°F), and 1427°C (2600°F). It has been shown that the pretest annealing temperature can have a pronounced effect on the creep-rupture properties at the test temperatures investigated. Strengths were progressively increased by pretest anneals at increasing temperatures up to approximately 1593°C (2900°F). With higher pretest annealing temperatures, inferior strength and ductility are observed. A tentative explanation of this behavior in terms of the distribution of precipitates in the alloy is offered. The improved properties resulting from a 1-hr pretest anneal at 1593°C (2900°F) are shown to be stable for at least 1000 hr at 982°C (1800°F) and 1204°C (2200°F). These improvements are achieved at the expense of a significant but not prohibitive reduction in ductility. In view of the pronounced curvature of some of the creep-rupture curves at long times, it is concluded that very short-time data frequently do not provide an adequate evaluation of an alloy.

ACKNOWLEDGMENTS

The author wishes to acknowledge the contributions made to this work by others. Those who merit specific mention are J. R. Weir for guidance and suggestions during the course of this work, E. R. Boyd and C. W. Houck for the preparation of metallographic specimens, C. K. Thomas for performance of the experimental details and the Metals and Ceramics Division Reports Office for the preparation of this report.

---

[4]T. E. Wilmarth, private communication.

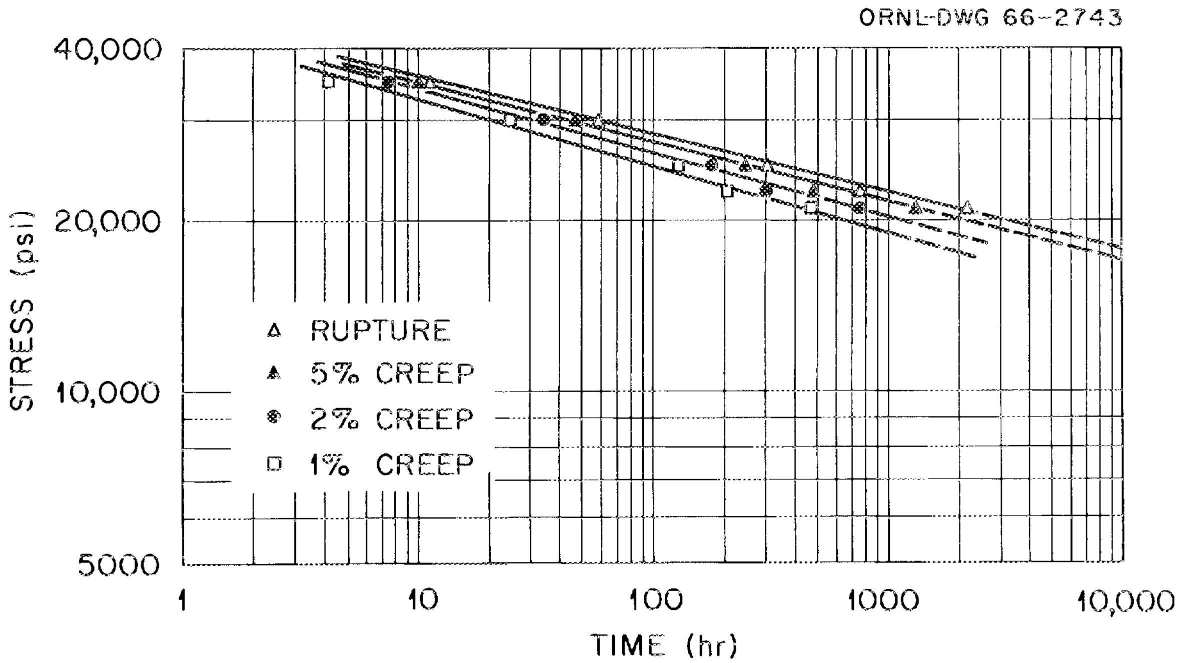

Fig. 1. Creep-Rupture Properties of FS-85 Alloy at 982°C (1800°F).

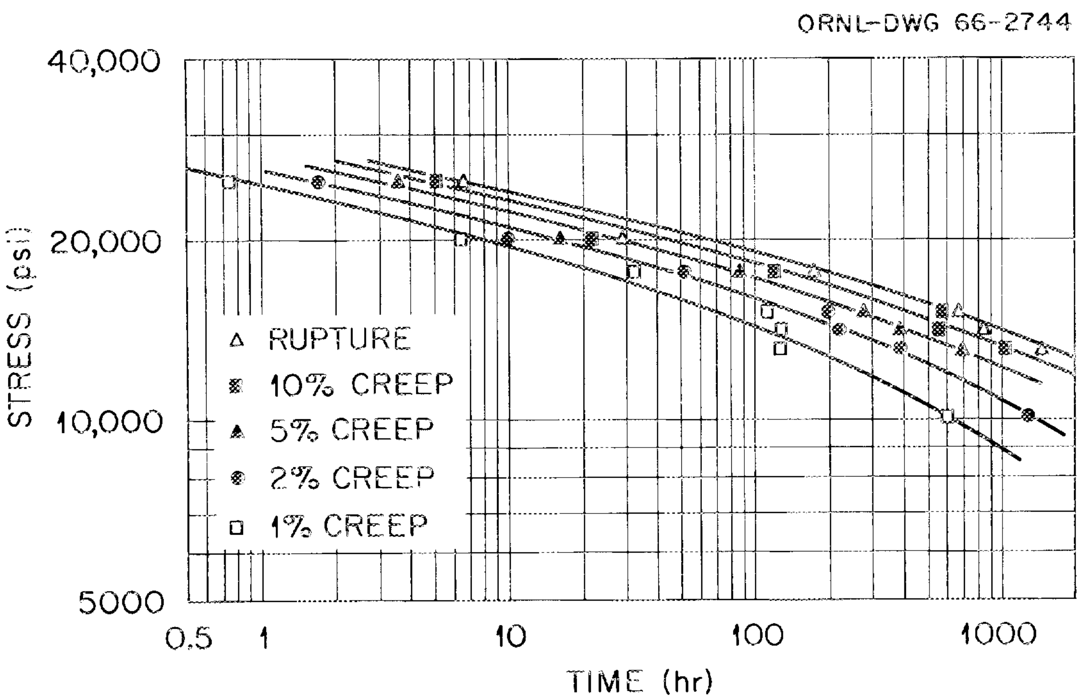

Fig. 2. Creep-Rupture Properties of FS-85 Alloy at 982°C (1800°F).

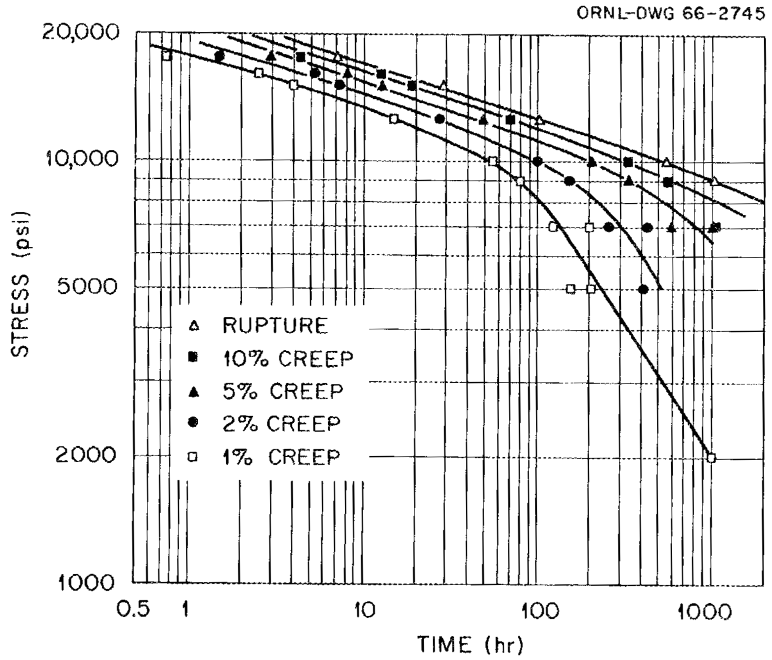

Fig. 3. Creep-Rupture Properties of FS-85 Alloy at 1204°C (2200°F).

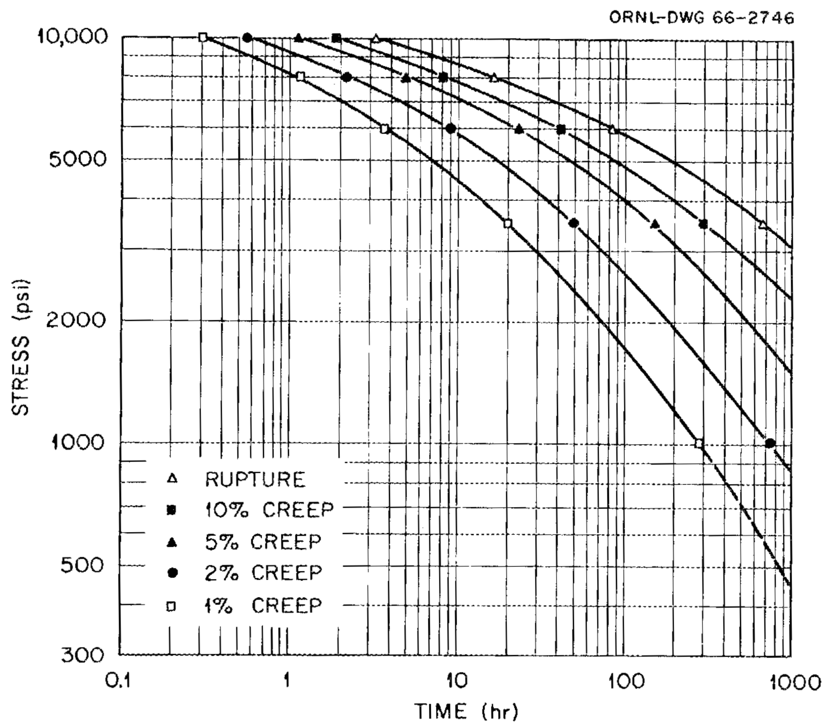

Fig. 4. Creep-Rupture Properties of FS-85 Alloy at 1427°C (2600°F).

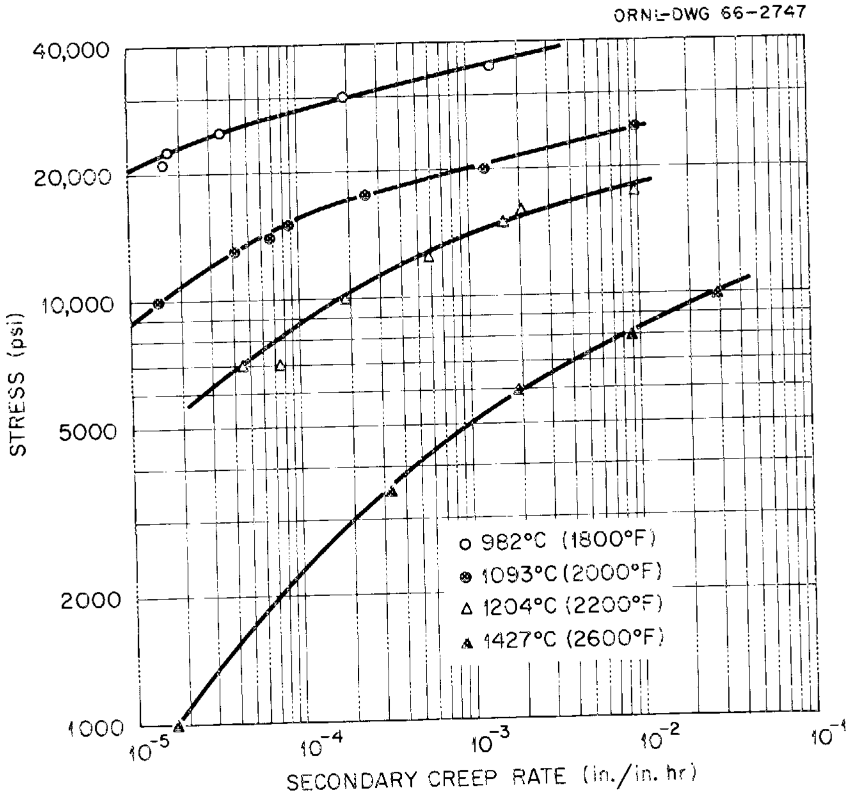

Fig. 5. Secondary Creep Rate vs Stress for FS-85 Alloy.

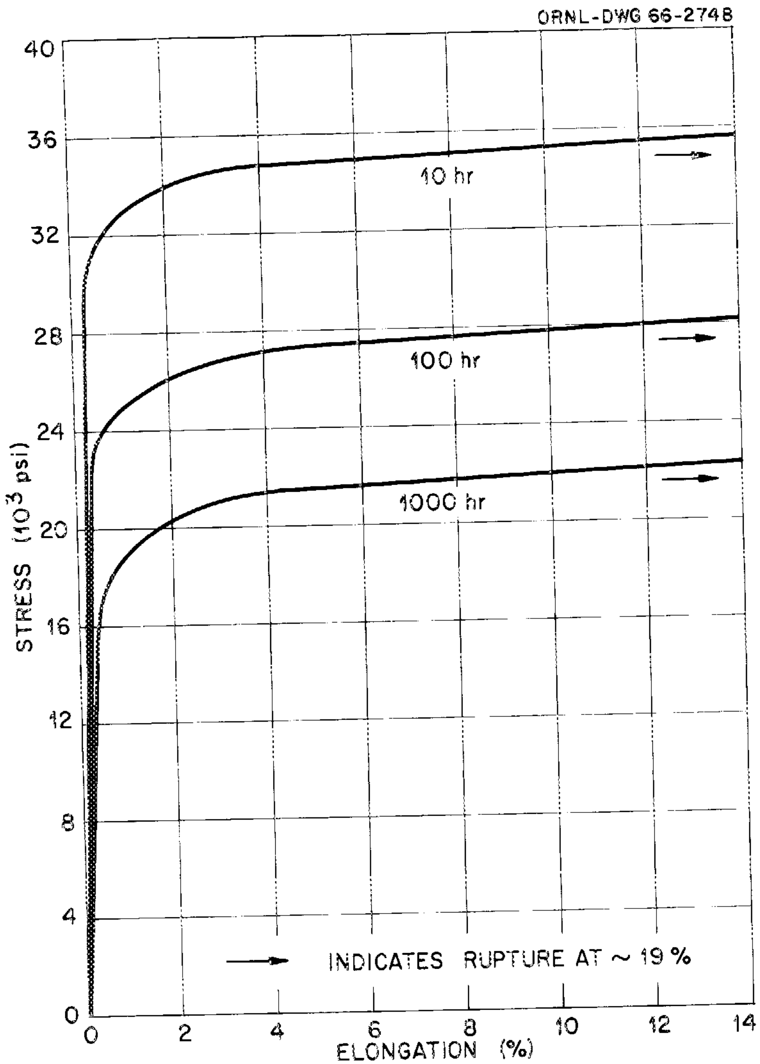

Fig. 6. Isochronous Stress-Strain Curves for FS-85 at 980°C (1800°F).

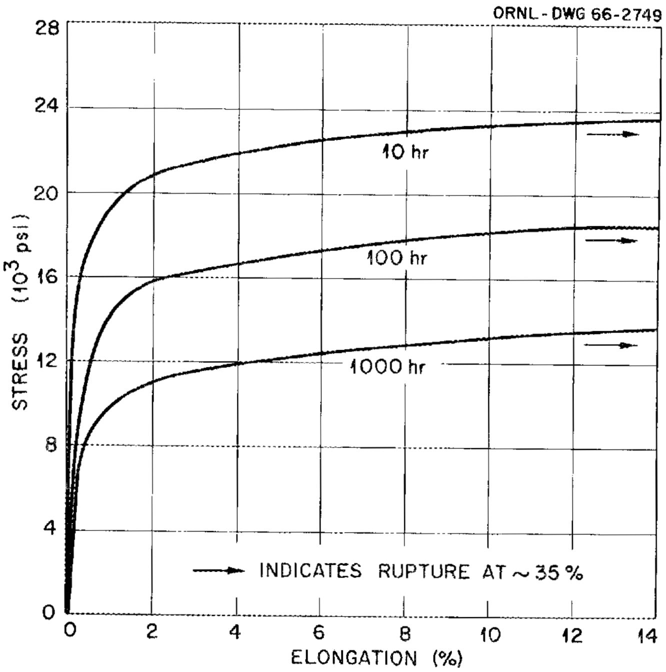

Fig. 7. Isochronous Stress-Strain Curves for FS-85 at 1900°C (2000°F).

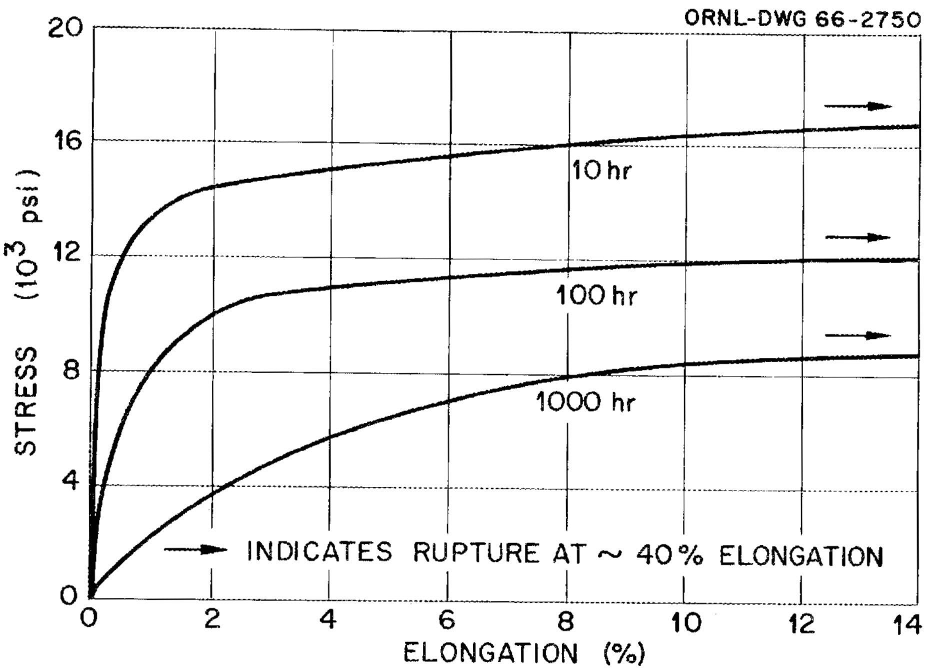

Fig. 8. Isochronous Stress-Strain Curves for FS-85 at 1204°C (2200°F).

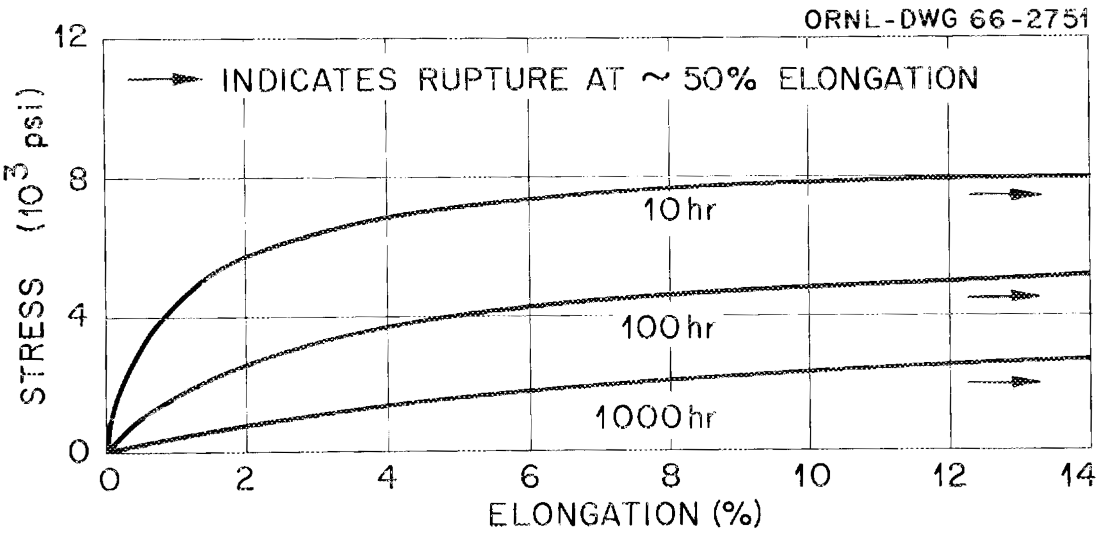

Fig. 9. Isochronous Stress-Strain Curves for FS-85 at 1427°C (2600°F).

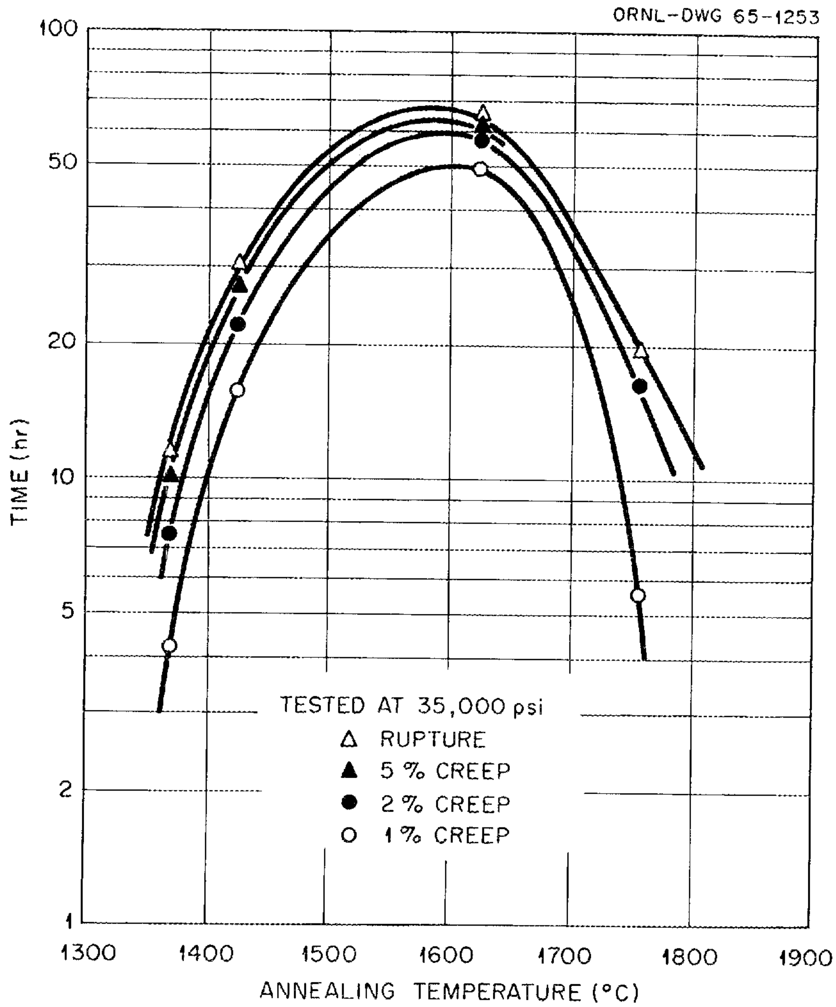

Fig. 10. Effect of Annealing Temperature on Creep-Rupture Properties of FS-85 Alloy at 980°C.

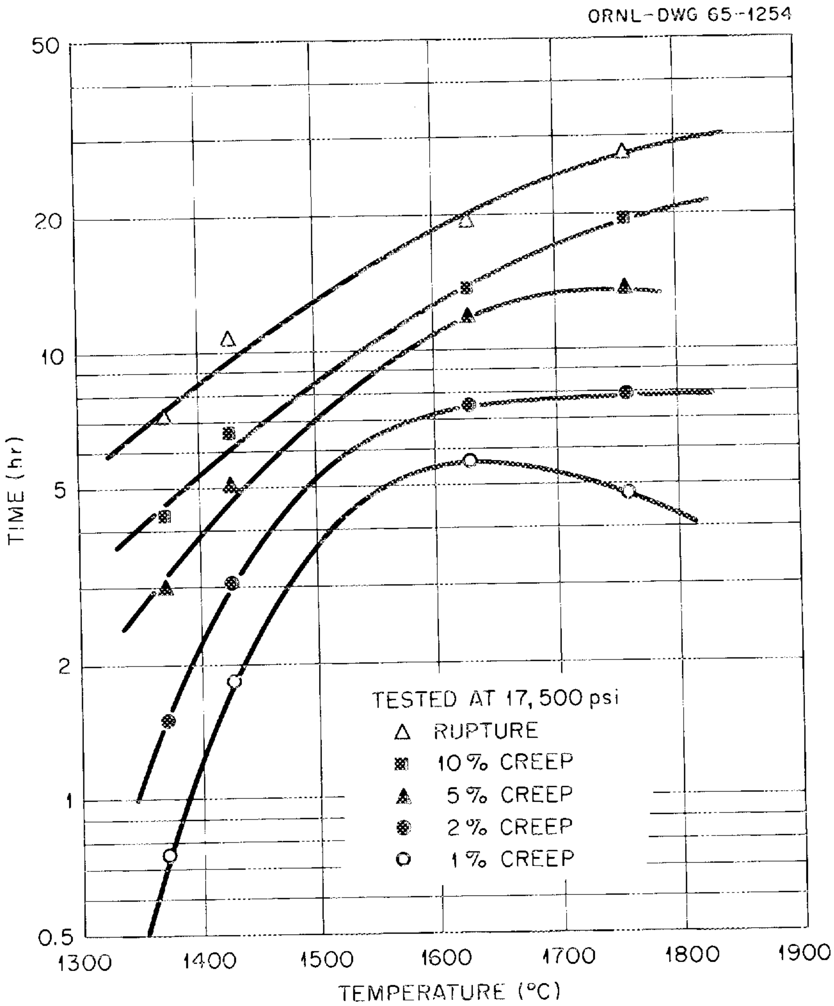

Fig. 11. Effect of Annealing Temperature on Creep-Rupture Properties of FS-85 Alloy at 1204°C.

ORNL-DWG 66-2752

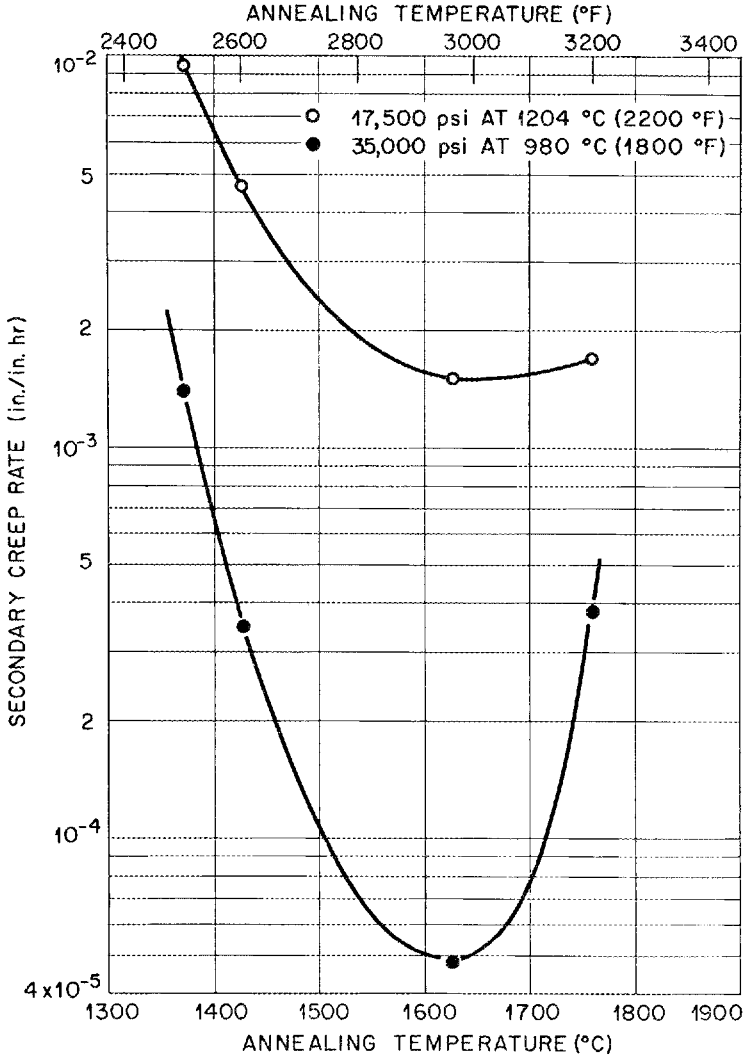

Fig. 12. Effect of Pretest Annealing Temperature on the Secondary Creep Rate of FS-85.

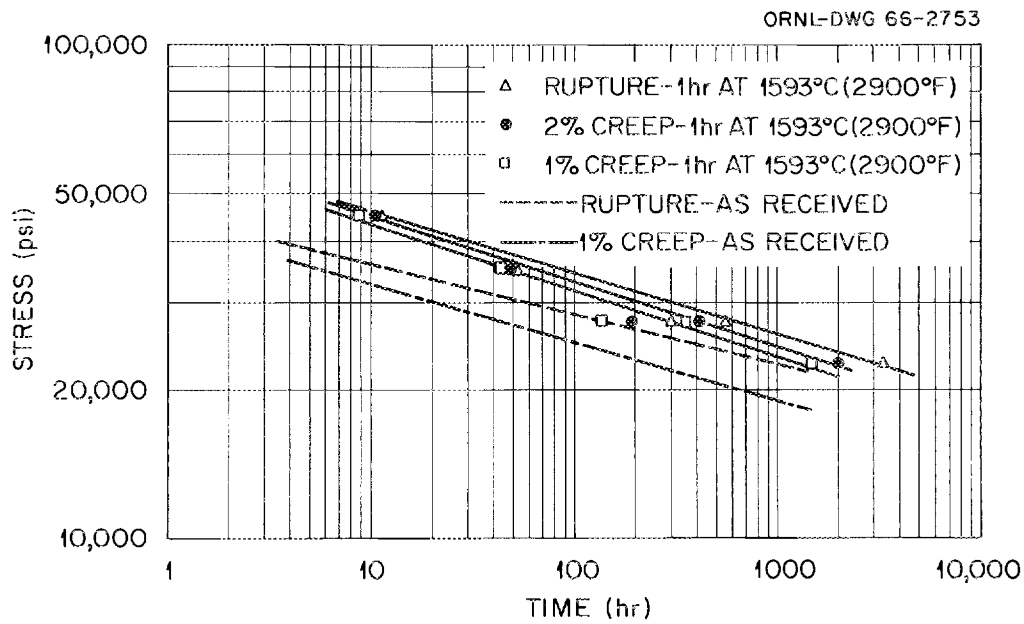

Fig. 13. Creep-Rupture Properties of Pretest-Annealed FS-85 at 982°C (1800°F).

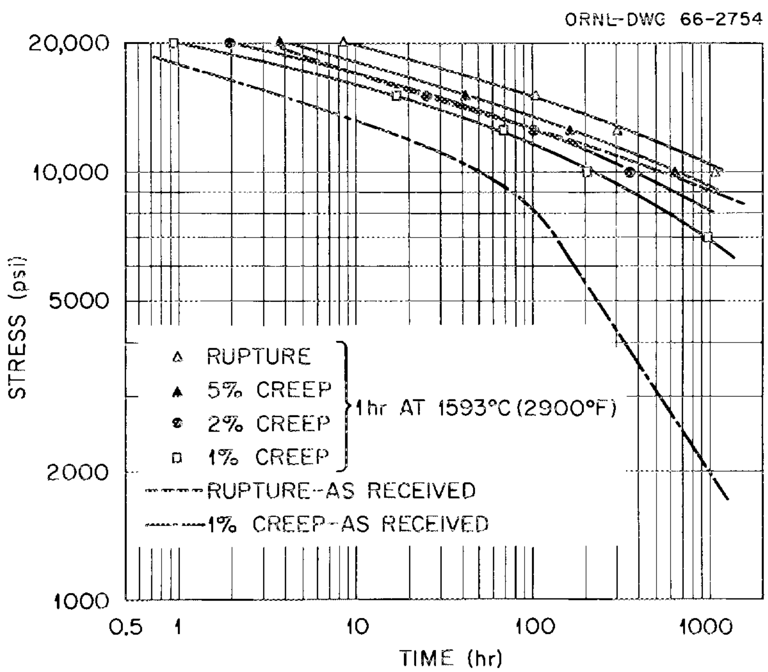

Fig. 14. Creep-Rupture Properties of Pretest-Annealed FS-85 at 1204°C (2200°F).

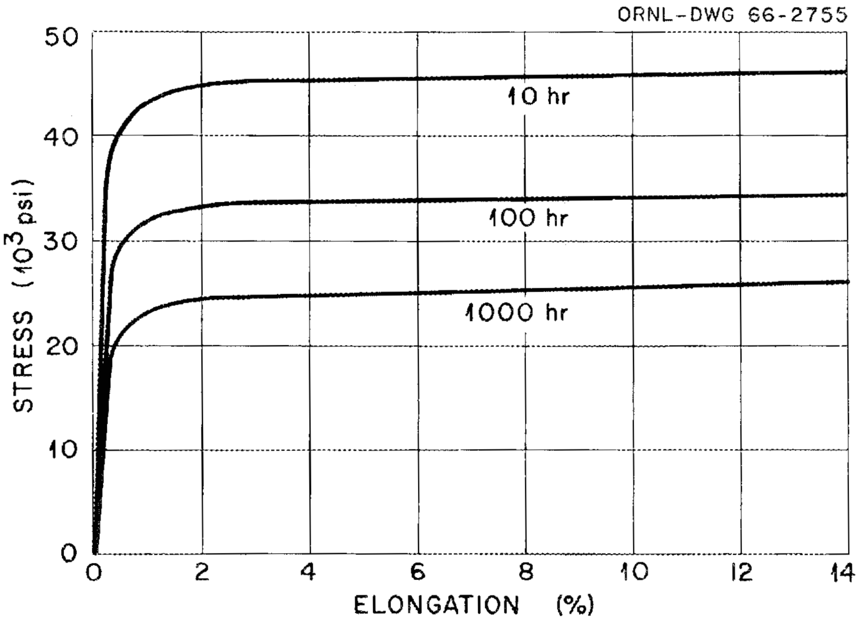

Fig. 15. Isochronous Stress-Strain Curves for Pretest-Annealed FS-85 at 982°C (1800°F).

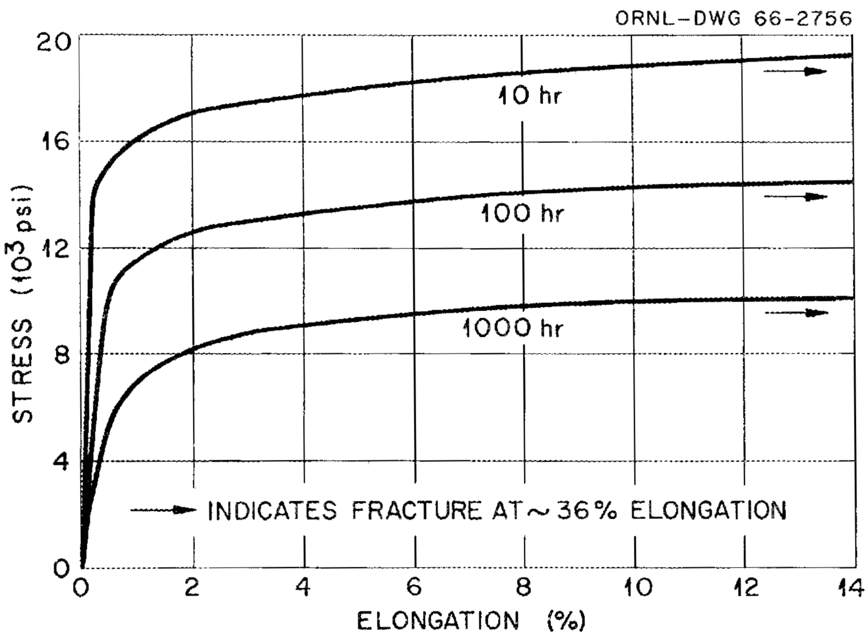

Fig. 16. Isochronous Stress-Strain Curves for Pretest-Annealed FS-85 at 1204°C (2200°F).

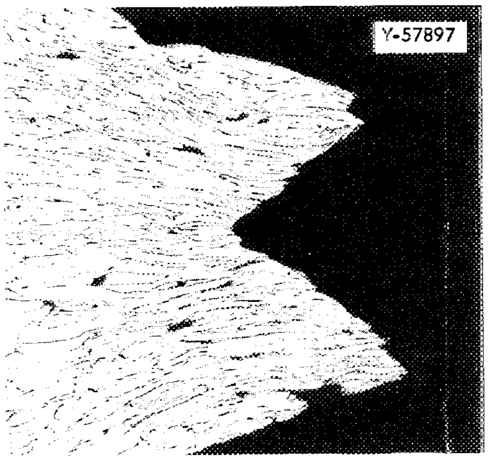

100×

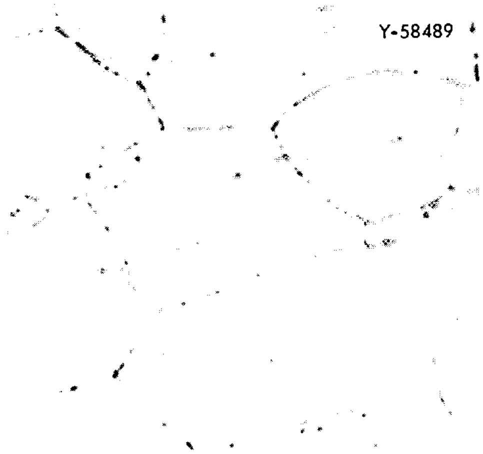

1000×

(a) 11.2 hr.

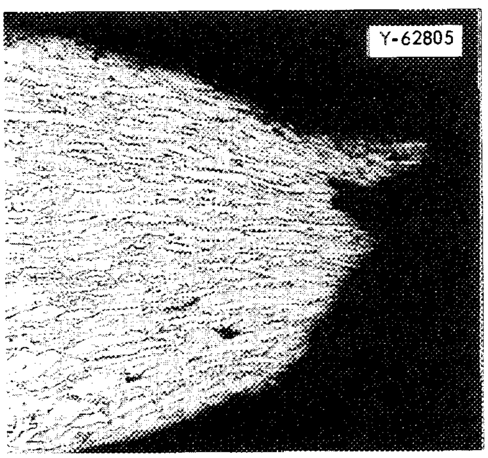

100×

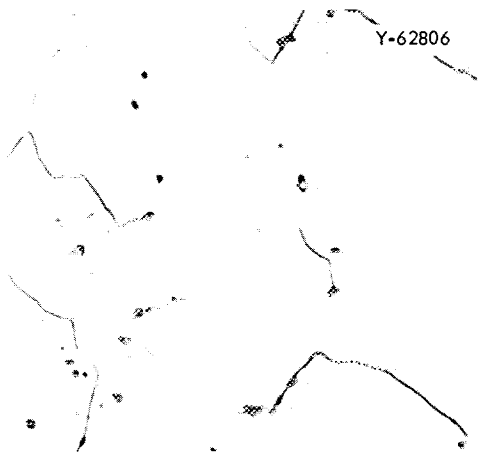

1000×

(b) 2240.2 hr

Fig. 17. Photomicrographs of Specimens Tested at 982°C (1800°F).

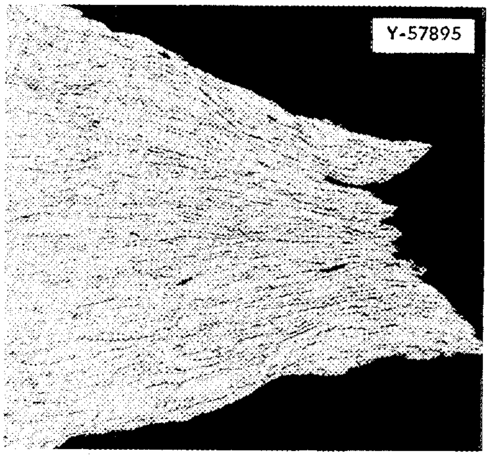

100×

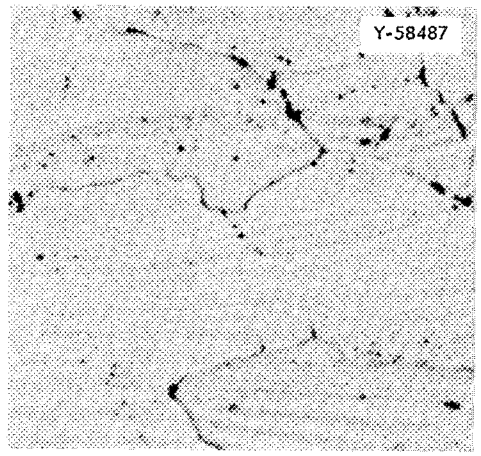

1000×

(a) 29.1 hr

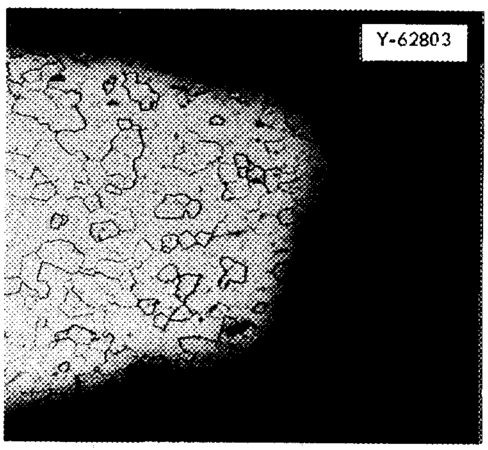

100×

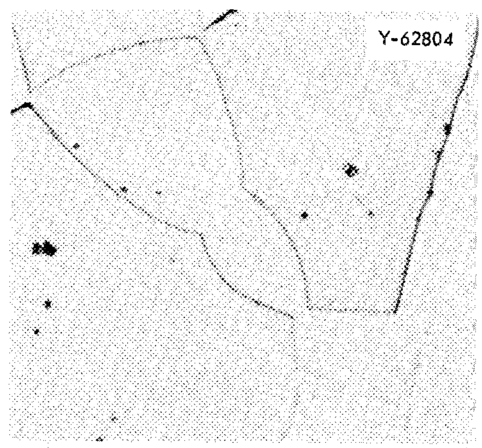

1000×

(b) 1452.7 hr

Fig. 18. Photomicrographs of Specimens Tested at 1093°C (2000°F).

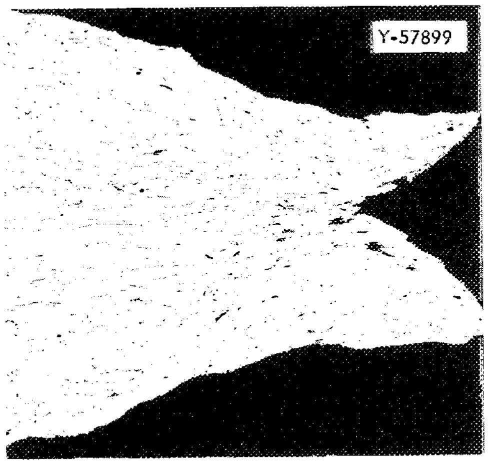

100×

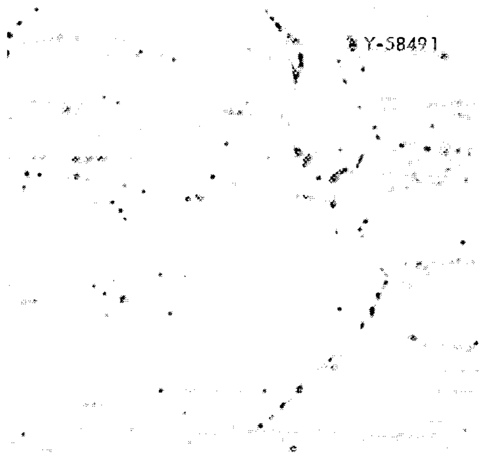

1000×

(a) 7.1 hr

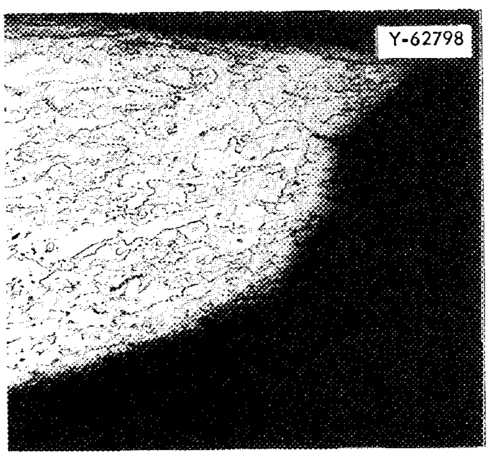

100×

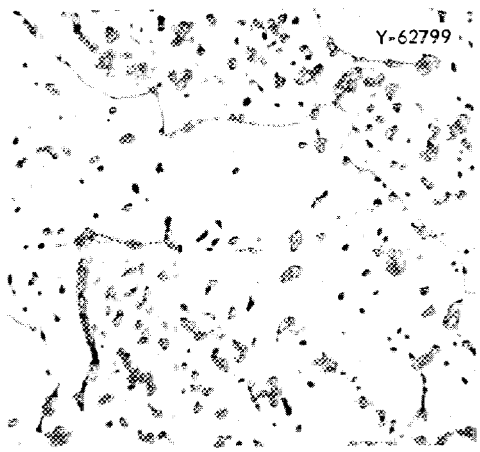

1000×

(b) 1033.9 hr

Fig. 19. Photomicrographs of Specimens Tested at 1204°C (2200°F).

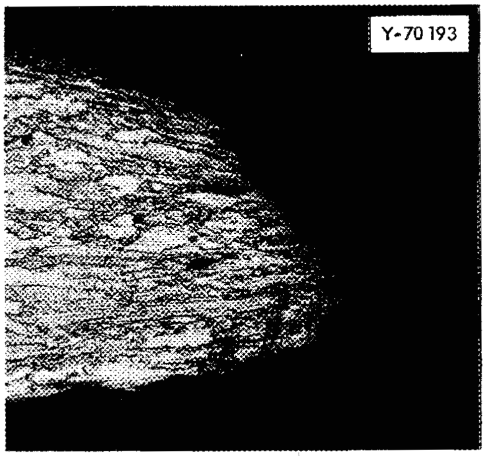

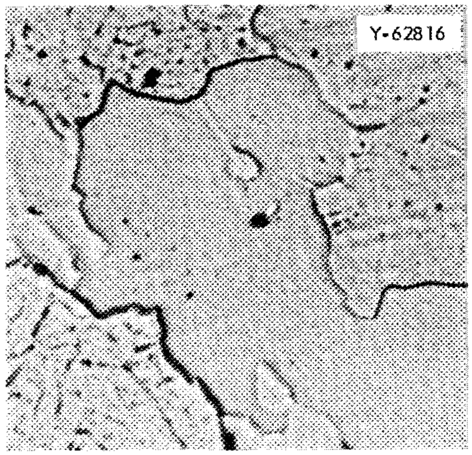

100×　　　　1000×

(a) 16.1 hr

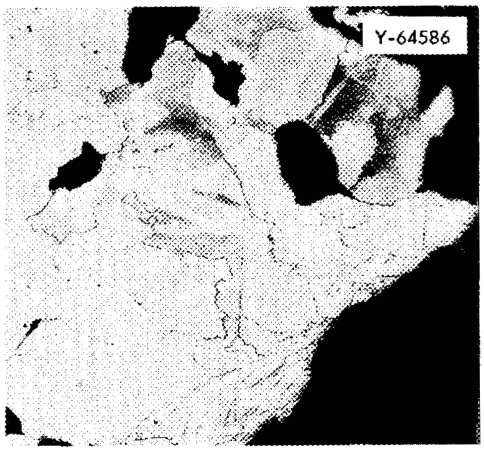

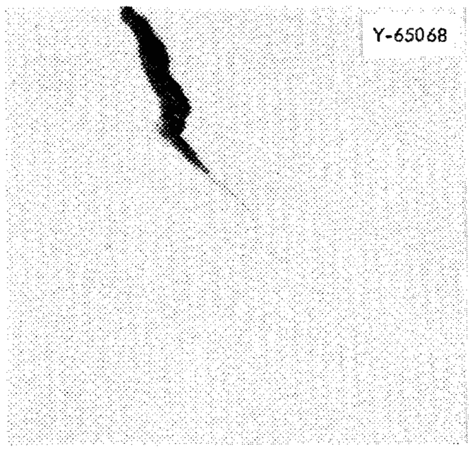

100×　　　　1000×

(b) 669.9 hr

Fig. 20. Photomicrographs of Specimens Tested at 1427°C (2600°F).

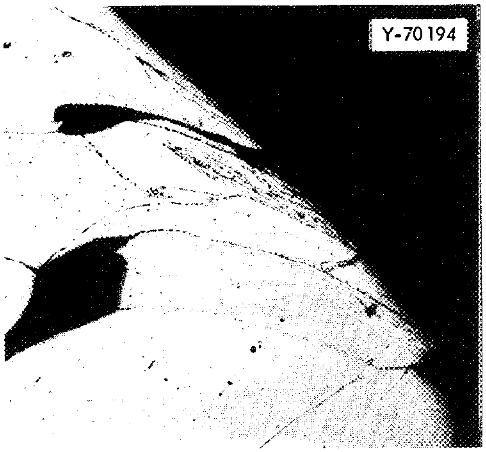

100×

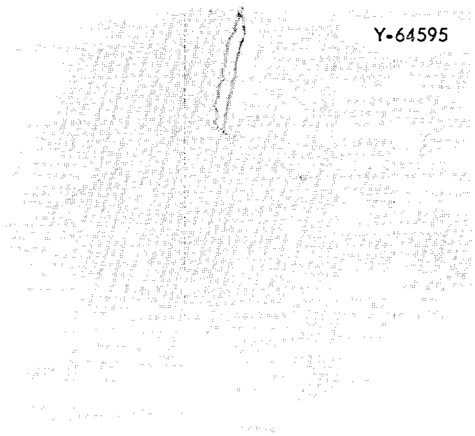

500×

(a) 12.0 hr at 982°C (1800°F)

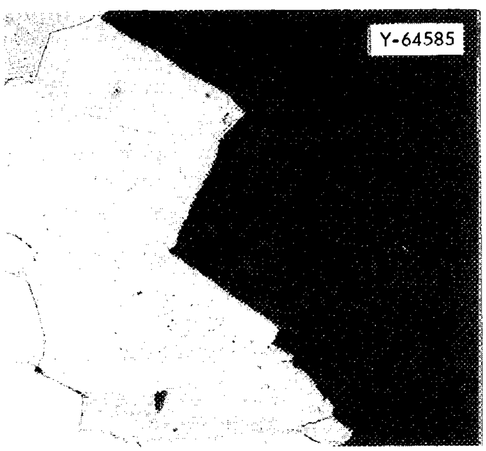

100×

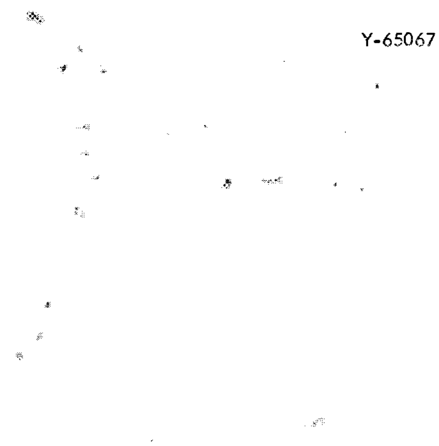

1000×

(b) 27.6 hr at 1204°C (2200°F)

Fig. 21. Photomicrographs of Specimens Tested After Pretest Annealing at 1760°C (3200°F).

INTERNAL DISTRIBUTION

1–3. Central Research Library
4–5. ORNL – Y-12 Technical Library
Document Reference Section
6–15. Laboratory Records
16. Laboratory Records, ORNL R.C.
17. ORNL Patent Office
18. G. M. Adamson, Jr.
19. S. E. Beall
20. D. T. Bourgette
21. G. E. Boyd
22. D. A. Canonico
23. K. V. Cook
24. F. L. Culler
25. C. A. Cunningham
26. J. E. Cunningham
27. J. H. DeVan
28. J. H. DiStefano
29. R. G. Donnelly
30. D. A. Douglas
31. W. S. Ernst
32. J. I. Federer
33. A. P. Fraas
34. E. A. Franco-Ferreira
35. J. H Frye, Jr.
36. L. C. Fuller
37. J. M. Googin (Y-12)
38. W. R. Grimes
39. A. G. Grindell
40. W. O. Harms
41. R. L. Heestand
42–44. M. R. Hill
45. H. W. Hoffman
46. W. R. Huntley
47. H. Inouye
48. D. H. Jansen
49. W. H. Jordan
50. G. W. Keilholtz
51. C. E. Larson (K-25)
52. C. F. Leitten, Jr.
53. A. P. Litman
54. R. N. Lyon
55. H. G. MacPherson
56. R. E. MacPherson
57. R. W. McClung
58. H. E. McCoy
59. R. E. McDonald
60. D. L. McElroy
61. F. R. McQuilkin
62. A. J. Miller
63. R. E. Moore
64. M. F. Osborne
65. P. Patriarca
66. F. H. Patterson
67. G. A. Reimann
68. W. C. Robinson, Jr.
69. A. W. Savolainen
70. J. E. Savolainen
71. J. L. Scott
72. A. C. Schaffhauser
73. C. E. Sessions
74. G. M. Slaughter
75. S. H. Smiley (K-25)
76–90. R. L. Stephenson
91. J. E. Strain
92. R. W. Swindeman
93. S. C. Weaver
94. A. M. Weinberg
95. J. R. Weir
96. H. C. Young
97. J. Zasler

EXTERNAL DISTRIBUTION

98. G. M. Anderson, AEC Washington
99. C. H. Armbruster, Wright-Patterson AFB
100–102. V. P. Calkins, General Electric, NMPO
103. S. S. Christopher, Combustion Engineering, Inc.
104–106. D. F. Cope, AEC, Oak Ridge Operations Office
107. J.W.R. Creagh, NASA, Lewis Research Center
108. J. Davis, Jet Propulsion Laboratory
109. R. W. Dayton, Battelle Memorial Institute
110. G. K. Dicker, AEC, Washington
111. E. M. Douthett, AEC, Washington
112. J. K. Elbaum, Code MAMP, Wright-Patterson AFB
113. D. DeHalas, Pacific Northwest Laboratory, Richland
114. D. C. Goldberg, Westinghouse Astronuclear Laboratory
115–116. D. H. Gurinsky, Brookhaven National Laboratory
117. R. Hall, NASA, Lewis Research Center
118. R. C. Hamilton, Institute for Defense Analyses, 1666 Connecticut Avenue, N.W., Washington, D.C.
119. E. E. Hoffman, General Electric, Cincinnati
120. W. R. Holman, Lawrence Radiation Laboratory
121. C. Johnson, Space Nuclear Systems Division, Space Electric Power Office, AEC, Washington 20545
122. J. S. Kane, University of California
123. J. J. Lombardo, NASA, Lewis Research Center
124. J. J. Lynch, NASA, Washington
125. T. P. Moffitt, NASA, Lewis Research Center
126–128. T. A. Moss, NASA, Lewis Research Center
129. R. A. Noland, Argonne National Laboratory
130. Louis Rosenblum, NASA, Lewis Research Center
131. A. J. Rothman, Lawrence Radiation Laboratory
132. N. D. Sanders, NASA, Lewis Research Center
133. H. Schwartz, NASA, Lewis Research Center
134. F. C. Schwenk, AEC, Washington
135–139. J. M. Simmons, AEC, Washington
140. D. K. Stevens, AEC, Washington
141. G. W. Wensch, AEC, Washington
142. M. J. Whitman, AEC, Washington
143. Division of Research and Development, AEC, ORO
144–158. Division of Technical Information Extension